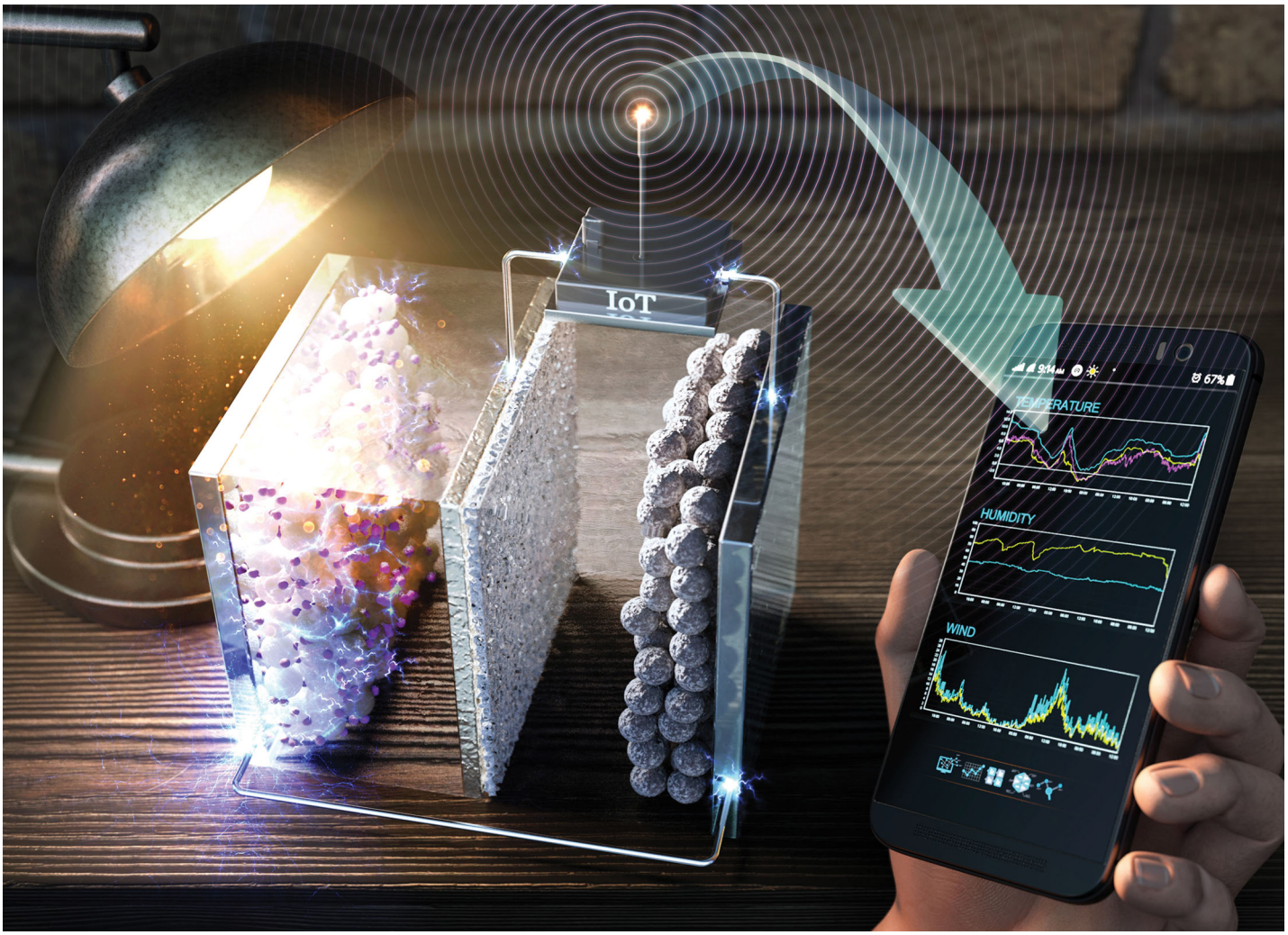

Showcasing research from Professor Hyun-Kon Song's laboratory, School of Energy and Chemical Engineering, Ulsan National Institute of Science and Technology, Ulsan, Korea.

Indoor-light-energy-harvesting dye-sensitized photo-rechargeable battery

Photo-rechargeable batteries (PRBs) benefit from their bifunctionality covering energy harvesting and storage. However, dim-light performances of the PRBs for indoor applications have not been illuminated. Herein, we present an external-power-free single-structured PRB named dye-sensitized photo-rechargeable battery (DSPB) with a light-to-charge energy efficiency of 11.5% in dim light. The successful operation of an IoT sensor by the DSPB under 1000 lux confirmed feasibility of the indoor-light-harvesting PRBs.

As featured in:

See Tae-Hyuk Kwon, Hyun-Kon Song *et al.*, *Energy Environ. Sci.*, 2020, **13**, 1473.

ROYAL SOCIETY OF CHEMISTRY

rsc.li/ees

Registered charity number: 207890

Energy & Environmental Science

ROYAL SOCIETY OF CHEMISTRY

PAPER

View Article Online
View Journal | View Issue

Cite this: *Energy Environ. Sci.*, 2020, **13**, 1473

Indoor-light-energy-harvesting dye-sensitized photo-rechargeable battery†

Byung-Man Kim,‡[a] Myeong-Hee Lee,‡[b] Vijayan Sobhana Dilimon,[b] Jeong Soo Kim,[a] Jung Seung Nam,[a] Yoon-Gyo Cho,[b] Hyun Kuk Noh,[b] Deok-Ho Roh,[a] Tae-Hyuk Kwon *[a] and Hyun-Kon Song *[b]

Received 9th October 2019,
Accepted 28th November 2019

DOI: 10.1039/c9ee03245b

rsc.li/ees

Photo-rechargeable batteries (PRBs) benefit from their bifunctionality covering energy harvesting and storage. However, dim-light performances of the PRBs for indoor applications have not been reported. Herein, we present an external-power-free single-structured PRB named a dye-sensitized photo-rechargeable battery (DSPB) with an outstanding light-to-charge energy efficiency ($\eta_{overall}$) of 11.5% under the dim light condition. This unprecedented $\eta_{overall}$ was attributed to the thermodynamically-favorable design of the DSPB that maximizes the working potential. At high-power irradiation, the kinetically-fast but thermodynamically-unfavorable iodine mediator (I^-/I_3^-) showed the highest charge and discharge capacities even if its discharge voltage was lowest. Under dim-light for indoor applications, however, the thermodynamically-favorable but kinetically-slow copper complex mediator ($Cu^{+/2+}(dmp)_2$) showed energy density and efficiency superior to I^-/I_3^- because its kinetics did not limit the harvesting capacity. The successful demonstration of the ability of the DSPB to operate a temperature-sensing IoT device only by indoor light opens the possibility of realizing indoor-light-harvesting PRBs.

Broader context

Buildings account for approximately 40% of world energy consumption. Building energy management system industries have been rapidly growing to improve the energy efficiency of buildings for reducing carbon emission. Wireless sensors and controllers connected to the internet (internet of things or IoT) play an important role in the building management system by monitoring and controlling the indoor conditions. The wireless IoT devices powered by batteries require cumbersome battery replacement. Therefore, a photovoltaic power supply is considered to be most ideal for the wireless devices but only if the indoor dim light could generate enough power to operate the devices. Here, we present a photo-rechargeable battery, which successfully operated a wireless IoT sensor by using low-intensity indoor light. The indoor photo-rechargeable battery is a device that can integrate both energy harvesting and storage, which should be distinguished from indoor solar cells.

Introduction

Internet-of-things devices and sensor networks are becoming widespread in our daily life and smart factories. Batteries have been used to supply power to the devices to overcome the limited reach of grid power connection. However, batteries have to be replaced or recharged by grid electricity after their stored energy gets exhausted. Photo-rechargeable batteries (PRBs) have been designed to have bifunctionality of photo-energy harvesting and storage integrated in a single structure.[1,2] Photo-excited electrons are stored in electric double layers or reduced chemical species.[3,4] As an example, a PRB could be designed to be photo-charged by a photo-anodic process and a cathodic process of an electroactive species. PRBs do not require electro-charging so they are expected to be one of the promising indoor power suppliers to overcome the limitation of conventional batteries.[5–7] However, dim-light performances of the PRBs for indoor applications have not been reported.

To achieve a high energy density of a PRB under dim light conditions, it is first necessary to increase (1) the gap of the reduction potential between the electroactive species on the photo-electrode and the storage-electrode and then (2) the charge densities (concentration) of the electroactive species. Charge and

[a] *Department of Chemistry, Ulsan National Institute of Science & Technology, Ulsan 44919, Korea. E-mail: kwon90@unist.ac.kr*
[b] *School of Energy and Chemical Engineering, Ulsan National Institute of Science & Technology, Ulsan 44919, Korea. E-mail: philiphobi@hotmail.com*

† Electronic supplementary information (ESI) available. See DOI: 10.1039/c9ee03245b

‡ These authors contributed equally.

mass transfer kinetics is not as important as the thermodynamic gap (therefore, the kinetics is the second consideration) because the photo-excitation process under dim light irradiation is slow enough to limit the overall kinetics. The dye-sensitized photo-electrodes have been most popularly employed for harvesting solar energy in PRBs. Especially, they are a promising candidate for indoor light-energy conversion because dye-sensitized solar cells (DSSCs) have been demonstrated to be superior to other photovoltaics such as silicon and organic solar cells under low light intensity.[8–10] Although the reduction potential of the redox mediator in the photo-electrode compartment is allowed up to the HOMO level of the dye molecule (*e.g.*, +1.08 V *versus* NHE (V_{NHE}) for Y123), only the iodine mediator (I^-/I_3^-) at +0.4 V_{NHE} (much more negative than the HOMO level) has been employed in the dye-sensitized photo-electrodes of PRBs. We have a large margin to increase the reduction potential of the mediator and therefore to increase the overall cell potential. From the viewpoint of the charge density, on the other hand, an electroactive species soluble in the electrolyte in the storage-electrode compartment (*e.g.*, S_4^{2-}/S_2^{2-}, $V^{3+/2+}$ and $C_8H_6N_2^{0/x-}$ [11–13]) would not be preferred since insoluble solid electroactive materials immobilized on the electrode (*e.g.*, $WO_3^{0/x-}$ and polypyrrole$^{x+/0}$ [14,15]) are expected to exhibit higher charge densities. It is difficult to reach charge densities higher than 1000 C cm^{-3} using soluble electroactive species: 580 C cm^{-3} for 3 M S_4^{2-}/S_2^{2-} (soluble) and 10 C cm^{-3} for 0.1 M $C_8H_6N_2^{0/x-}$ (soluble; $x = 1$ assumed) *versus* 1500 C cm^{-3} for $WO_3^{0/x-}$ (insoluble; $x = 0.5$ assumed).[11,13,14]

Single-structured PRBs have generally employed capacitive storage rather than battery-type storage. The mismatch of potential level between the photo-electrode and active materials of lithium ion batteries (LIBs) was the main concern:[16–18] the reduction potentials of anode materials are too negative to accept charge from the photo-electrode while those of cathode materials are too positive to achieve a high working potential during discharge. Instead of single structures, photo-rechargeable systems have been realized by a wire connecting a LIB to a photovoltaic pack having multiple photovoltaic cells in series (two devices in a system).[19–22] The hybrid battery–photovoltaic systems suffer from a bulky design, overcharge risk and energy loss due to wire connection.[17,18] For indoor applications, therefore, single-structured PRBs are expected to be superior to the two devices in a system. Also, photo-assisted rechargeable batteries have been proposed, in which photo-energy was used only to reduce external-power consumption during charging.[23–27] However, they are far away from self-rechargeable systems.

In this work, we present an external-power-free single-structured PRB (named a dye-sensitized photo-rechargeable battery or DSPB) especially designed for indoor light energy harvesting. The DSPB was designed to be photo-charged by the photo-anodic process of DSSCs and the cathodic process of LIBs. The extra lithium insertion reaction of $LiMn_2O_4$ spinel to $Li_2Mn_2O_4$ at +3.0 $V_{Li+/Li}$ (V *versus* Li^+/Li) was carefully selected as the cathodic process on the storage-electrode. The $Mn^{4+/3+}$ electrochemistry has a high charge density at 2300 C cm^{-3} at the reduction potential appropriate for operating the PRB. The instability of the reaction was overcome by wrapping the $LiMn_2O_4$ particles with a few layers of graphene (LMO@Gn). DSPB performances were strongly dependent on the thermodynamic and kinetic properties of the mediators. Under high-power irradiation, the kinetics of charge and/or mass transfer of the mediator determined the overall DSPB performances. Under the low-power irradiation of indoor lights, however, the reduction potential of the mediator (thermodynamics) determined the performances in terms of photo-charging energy density and overall efficiency because its kinetics did not limit the harvesting capacity. We demonstrated a successful operation of the DSPB based on a kinetically slow but high potential copper complex mediator ($Cu^{+/2+}(dmp)_2$) and the $LiMn_2O_4$-to-$Li_2Mn_2O_4$ reaction only using indoor light.

Results and discussion

Working principle

The DSPB consisted of three electrodes (Fig. 1a): a photo-electrode (PE), a storage electrode (SE) and an auxiliary discharge electrode (DE). Dye-sensitized TiO_2 particles were loaded on a transparent conductive oxide electrode for the PE. The PE was constructed in the form of two layers of TiO_2 on fluorine-doped tin oxide (FTO) glass: electrolyte|4.0 μm-thick scattering layer of TiO_2 in >100 nm|3.5 μm-thick active layer of TiO_2 in 30 nm|FTO (Fig. S1, ESI†). Incident light passing through FTO excites the dye (or sensitizer) molecules immobilized on the nanoporous active layer. A portion of the light passing through the active layer was scattered by the second layer of TiO_2 and re-utilized in the active layer. The co-sensitizer system including Y123 and DN-F10 was employed for efficient light harvesting (Fig. 1b).[28,29]

During the photo-charging process, electrons of dye molecules are photo-excited from the highest occupied molecular orbital (HOMO) to the lowest unoccupied molecular orbital (LUMO). The photo-excited electrons are transferred to the conduction band of TiO_2 and then flow through an external circuit to the SE. The active material of the SE, lithium manganese oxide spinel ($LiMn_2O_4$ or LMO) wrapped with a-few-layer graphene (LMO@Gn), is reduced by accepting the electrons from the PE *via*:

$$LiMn(III)Mn(IV)O_4 + Li^+ + e^- \rightarrow Li_2Mn(III)Mn(III)O_4 \quad (1)$$

The mediator (M_{red}) in the compartment of the PE donates electrons to regenerate the photo-oxidized dye molecules (D_{ox}) (Fig. 1b):[30]

$$M_{red} \rightarrow M_{ox} + ne^- \quad (2)$$

$$D_{ox} + e^- \rightarrow D_{red} \quad (3)$$

The photo-charging process proceeds until all molecules of the active materials of the SE are completely reduced or all the mediator molecules are completely oxidized. Overcharge is not allowed because the dye is regenerated only by the mediator oxidation (eqn (2) and (3)).

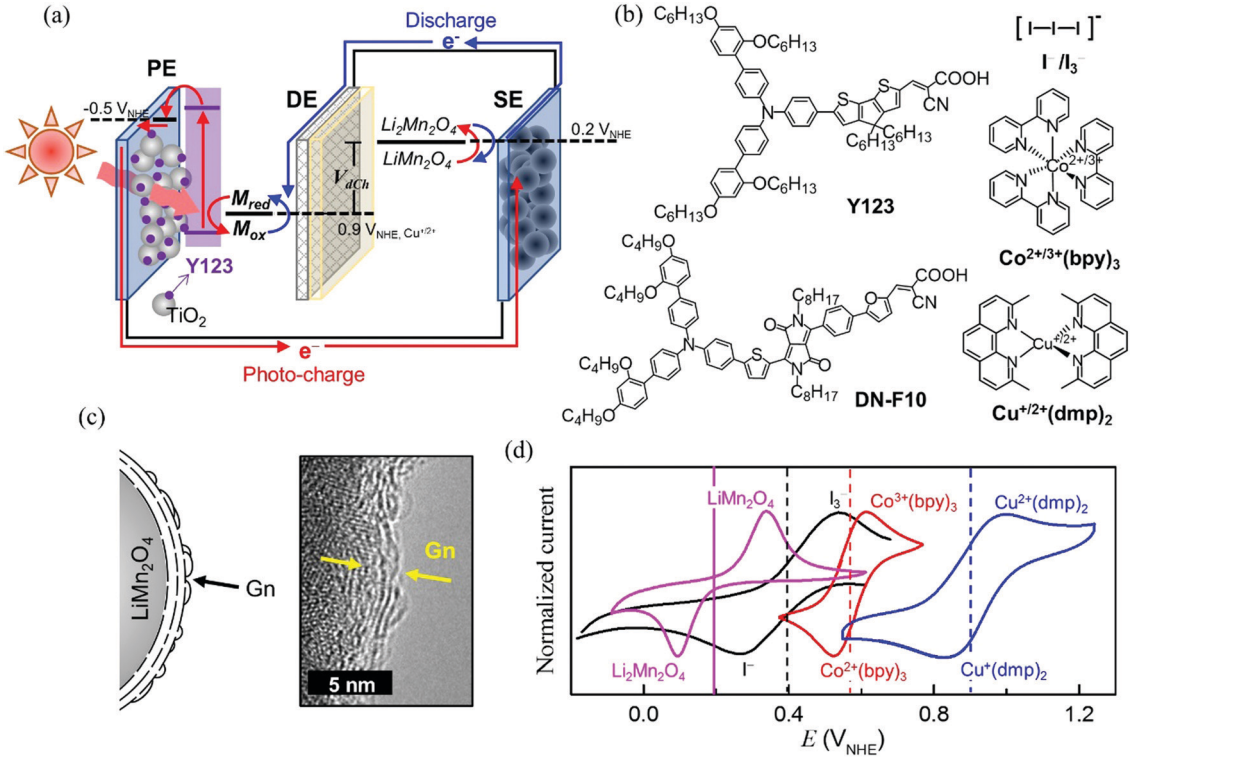

Fig. 1 DSPB. (a) Working principle. Different electrolytes were used for the PE and the SE, respectively: a mediator in acetonitrile for the PE and 0.8 M $LiClO_4$ in acetonitrile for the SE. (b) Molecular structures of dyes (Y123 and DN-F10) and mediators (I^-/I_3^-, $Co^{2+/3+}(bpy)_3$ and $Cu^{+/2+}(dmp)_2$). (c) Transmission electron microscopic images of LMO@Gn. (d) Cyclic voltammograms of active materials for energy storage in 0.1 M $LiClO_4$ in acetonitrile. The mediator is oxidized ($I^- \rightarrow I_3^-$; $Co^{2+}(bpy)_3 \rightarrow Co^{3+}(bpy)_3$; or $Cu^+(dmp)_2 \rightarrow Cu^{2+}(dmp)_2$) and LMO@Gn is reduced ($LiMn_2O_4 \rightarrow Li_2Mn_2O_4$) for energy storage by photo-charging.

Different electrolytes were used for the PE and the SE, respectively: a mediator in acetonitrile was used for the PE and 0.8 M $LiClO_4$ in acetonitrile was used for the SE. A Li^+-conductive oxide separator between the PE and the SE (lithium-ion conducting glass ceramic, LICGC™) does not allow ions except for Li^+ to transport between the compartments, blocking the mix-up of the electrolytes.[31] Therefore, the oxidized mediator molecules are not reduced on the counter electrode (the SE in DSPB), which distinguishes the DSPB from DSSCs. Photo-energy is stored as chemical energy in an oxidized form of the mediators of the PE (M_{ox}) and in a reduced form of the active material of the SE ($Li_2Mn_2O_4$). There is no possibility of overcharge problems because the Fermi level of TiO_2 limits the upper (or negative) potential cutoff of the active material of the SE.[12,32,33]

The discharging process proceeds between the SE and the DE without using the PE (Fig. 1a). The DE was made by depositing Pt metal on the PE-side of the Li^+-conductive separator in a stripe pattern (Fig. S2, ESI†). During the discharge, the reduced active material on the SE is oxidized (the backward reaction of eqn (1)) while the oxidized mediator is reduced to its reduced state on the DE (the backward reaction of eqn (2)). As a summary, the PE works as the photo-anode during photo-charging while the DE is the cathode for mediator reduction during discharge. The SE is used in both charge and discharge processes, acting as the cathode for charge and the anode for discharge processes.[30] The mediator in its reduced state (M_{red}) works as a charge regenerator during photo-charging while the oxidized mediator (M_{ox}) is the catholyte used to generate electricity.

LMO@Gn as a storage material

The working potential of the DSPB (V_{dCh}) is the potential difference between the redox mediator in the DE compartment and the active material of the SE ($V_{dCh} = V_{DE} - V_{SE}$). The reduction potential of the active material of the SE should be between the reduction potential of the redox mediator and the Fermi level of TiO_2. As high-energy-density storage materials, cathode or anode materials practically used in LIBs could be considered to be the active material of the SE. However, cathode materials used in LIBs (*e.g.*, $LiMn_2O_4$ spinel or LMO) are not appropriate since they are intrinsically reduced species and therefore they cannot be reduced. For example, LMO is oxidized at around +4.0 $V_{Li+/Li}$ (+1.0 V_{NHE}):

$$LiMn(III)Mn(IV)O_4 \rightarrow Mn(IV)Mn(IV)O_4 + Li^+ + e^- \quad (4)$$

Also, the reduction potential of the reaction is too positive to achieve a high working potential of the DSPB. On the other hand, the reduction potentials of anode materials of LIBs (*e.g.*, ~0 $V_{Li+/Li}$ or −3.0 V_{NHE}) are much more negative than the Fermi level of TiO_2. The active materials having very negative reduction potentials cannot accept electrons from TiO_2.

Therefore, neither cathode nor anode materials of LIBs can be used as the active material of the SE of the DSPB.

Instead of the anodic reaction of LMO at +4.0 $V_{Li+/Li}$ popularly used in LIBs, we used another cathodic reaction of LMO at ~+3.0 $V_{Li/Li+}$ or 0 V_{NHE} (eqn (1)) for the DSPB. The cathodic nature of the reaction and its reduction potential being more positive than the TiO_2 Fermi level satisfy the requirements of the active materials of the SE for the DSPB. However, unfortunately, the reversibility of the +3.0 $V_{Li+/Li}$ reaction has been reported to be very poor due to the Jahn–Teller distortion developed during the phase transition between the cubic phase of $LiMn_2O_4$ and the tetragonal phase of $Li_2Mn_2O_4$.[34] This limitation was overcome by nano-sizing and graphene-wrapping LMO particles (LMO@Gn in Fig. 1c and Fig. S3, ESI†).[35] 10 μm LMO particles were ground in the presence of graphite to form LMO@Gn in a significantly reduced size by using high-energy ball milling (Fig. S3b and c, ESI†). The crystallite size estimated from the (111) peak of XRD by the Scherrer equation was reduced from 135 nm for bare LMO to 63 nm for LMO@Gn (Fig. S3a, ESI†). The graphitic layer of LMO@Gn was identified by the X-ray diffraction peak at 26° and the transmission-electron-microscopic image (Fig. 1c). The LMO@Gn showed quasi-reversibility with long-term cyclability guaranteed (Fig. S4, ESI†).

Mediator-dependent DSPB performances

Three different molecules were tested as the mediator of DSPB: I^-/I_3^-, $Co^{2+/3+}(bpy)_3$ and $Cu^{+/2+}(dmp)_2$ (bpy = 2,2′-bipyridine; dmp = 2,9-dimethyl-1,10-phenanthroline; Fig. 1b).[36–40] The nanoparticular TiO_2 (30 nm in size) in the active layer of PE provides a porosity to allow diffusion of the metal complex mediators (ligand-to-ligand length = 1.2 nm) inside the porous active layer. From the thermodynamic standpoint, mediators were identified by their reduction potential (Fig. 1d). The reduction potential was measured by the average potential of cathodic and anodic peak potentials ($E_{1/2}$) of the cyclic voltammograms: $E_{1/2}$ = +0.92 V_{NHE} for $Cu^{+/2+}(dmp)_2$, +0.57 V_{NHE} for $Co^{2+/3+}(bpy)_3$ and +0.40 V_{NHE} for I^-/I_3^-. The mediators are appropriate for being paired with LMO@Gn for DSPBs since their $E_{1/2}$ were more positive than that of LMO@Gn (+0.2 V_{NHE}). A mediator of more positive reduction potential on DE makes a higher V_{dCh} of a DSPB cell. A higher energy density would be obtained from the cell at a higher V_{dCh} if the kinetics were facile enough to support the thermodynamic driving force. From the thermodynamic standpoint, therefore, $Cu^{+/2+}(dmp)_2$ was the best choice, followed by $Co^{2+/3+}(bpy)_3$ and I^-/I_3^-.

Unfortunately, however, the sluggish kinetics of the most-positive-potential mediator $Cu^{+/2+}(dmp)_2$ limited the photo-charging capacity (Q_{Ch}). DSPBs were photo-charged for 5 min under one sun condition (100 mW cm^{-2}; Fig. 2a), followed by being discharged galvanostatically (Fig. 2b). Photo-charging current (J_{Ch}) decreased with time as the reduced mediator was oxidized and $LiMn_2O_4$ was lithiated or reduced to $Li_2Mn_2O_4$.[41,42] The highest Q_{Ch} (calculated from the area below the chronoamperometric curves in Fig. 2a) was obtained from I^-/I_3^-, followed by $Co^{2+/3+}(bpy)_3$ and $Cu^{+/2+}(dmp)_2$: Q_{Ch} = 111 C cm^{-3} for I^-/I_3^-; 83.0 C cm^{-3} for $Co^{2+/3+}(bpy)_3$; and 38.6 C cm^{-3} for $Cu^{+/2+}(dmp)_2$. The Q_{Ch} and J_{Ch} of DSPBs based on $Cu^{+/2+}(dmp)_2$ were significantly lower than those of I^-/I_3^- and $Co^{2+/3+}(bpy)_3$, indicating the sluggish kinetics of $Cu^{+/2+}(dmp)_2$. The Q_{Ch} values of all mediators were fully utilized during discharge at 0.03 mA cm^{-2} without loss so that discharge capacity (Q_{dCh} in Fig. 2b) approached Q_{Ch}. Charge-to-discharge coulombic efficiency ($\eta_Q = Q_{dCh}/Q_{Ch}$) was estimated at ~100%, which was independent of mediators and light intensities (Fig. S5, ESI†). Therefore, Q_{dCh} was determined by the kinetics of mediators during photo-charging processes. The highest Q_{dCh} of I^-/I_3^- supported the highest discharge energy density (ED_{dCh} in Fig. 2c) even if its discharge potential is lowest: *e.g.*, ED_{dCh} = 7.8 mW h cm^{-3} at 100 mW cm^{-2}. Correspondingly, the light-to-charge energy efficiency ($\eta_{overall}$) of I^-/I_3^- was estimated at 0.53% (*cf.*, $\eta_{overall}$ = 0.39% for $Cu^{+/2+}(dmp)_2$), which is determined by $\eta_{overall} = (ED_{dCh}\,V)/(P_{in}At_{ch})$[20,43] with V = the volume of the active material (LMO@Gn) of SE, P_{in} = the incident light intensity, A = the electrode area of PE, and t_{Ch} = the photo-charging time. The overall efficiency $\eta_{overall}$ is the efficiency of the light-to-charge conversion process of the DSPB including the photon-to-electron conversion for energy harvesting (estimated by the power conversion efficiency, η_{PCE}) and the electron-to-discharged-chemical-energy conversion for energy storage and utilization (estimated by the storage efficiency, $\eta_{storage}$) (Fig. S6, ESI†): $\eta_{overall} = \eta_{PCE}\eta_{storage}$.

In addition to photo-charging, evidence of the sluggish kinetics of the dye regeneration process by mediators was found during discharge. The average discharge cell voltage (V_{dCh}) was 0.61 V for $Cu^{+/2+}(dmp)_2$, 0.36 V for $Co^{2+/3+}(bpy)_3$ and 0.26 V for I^-/I_3^- (Fig. 2b). The descending order of V_{dCh} followed that of $E_{1/2}$ of the mediators. The V_{dCh}–$E_{1/2}$ correspondence in their orders is easily understood since V_{dCh} is determined by the difference of $E_{1/2}$ between mediator and LMO@Gn ($\Delta E_{1/2,LMO}$). However, the V_{dCh} of $Cu^{+/2+}(dmp)_2$ having the highest reduction potential was significantly smaller than the corresponding $\Delta E_{1/2,LMO}$: V_{dCh} = 0.61 V *versus* $\Delta E_{1/2,LMO}$ = 0.72 V. A kinetic limitation causing polarization is expected from the smaller V_{dCh} for $Cu^{+/2+}(dmp)_2$. On the other hand, there appears to be insignificant kinetic polarization found in the presence of I^-/I_3^- and $Co^{2+/3+}(bpy)_3$ (V_{dCh} *versus* $\Delta E_{1/2,LMO}$ = 0.26 V *versus* 0.20 V for I^-/I_3^-, 0.36 V *versus* 0.37 V for $Co^{2+/3+}(bpy)_3$).

To correlate the cell-level kinetic limitation to the material-level properties of mediators, kinetic parameters were measured and compared (Fig. 3, Fig. S7, S8 and Table S1 (ESI†); Measurement and calculation details in the ESI†). The photo-charging current of the DSPB at the short circuit between PE and SE ($I_{sc,PE-SE}$) is determined by the light harvesting efficiency (η_{lh}), the charge injection efficiency (η_{inj}), the charge collection efficiency (η_{cc}) and the charge regeneration efficiency (η_{reg}):[44] $I_{sc,PE-SE} = qI_0\eta_{lh}\eta_{inj}\eta_{cc}\eta_{reg}$ with q = the elementary charge, and I_0 = the incident photon flux. The η_{reg}, a measure of how efficiently electrons are transferred from mediator molecules to dye molecules, is the single variable when mediators are varied and the electrode components and the dye of PE were fixed. The η_{reg} was measured by using the time-correlated-single-photon-counting technique. I^-/I_3^- showed the highest efficiency at

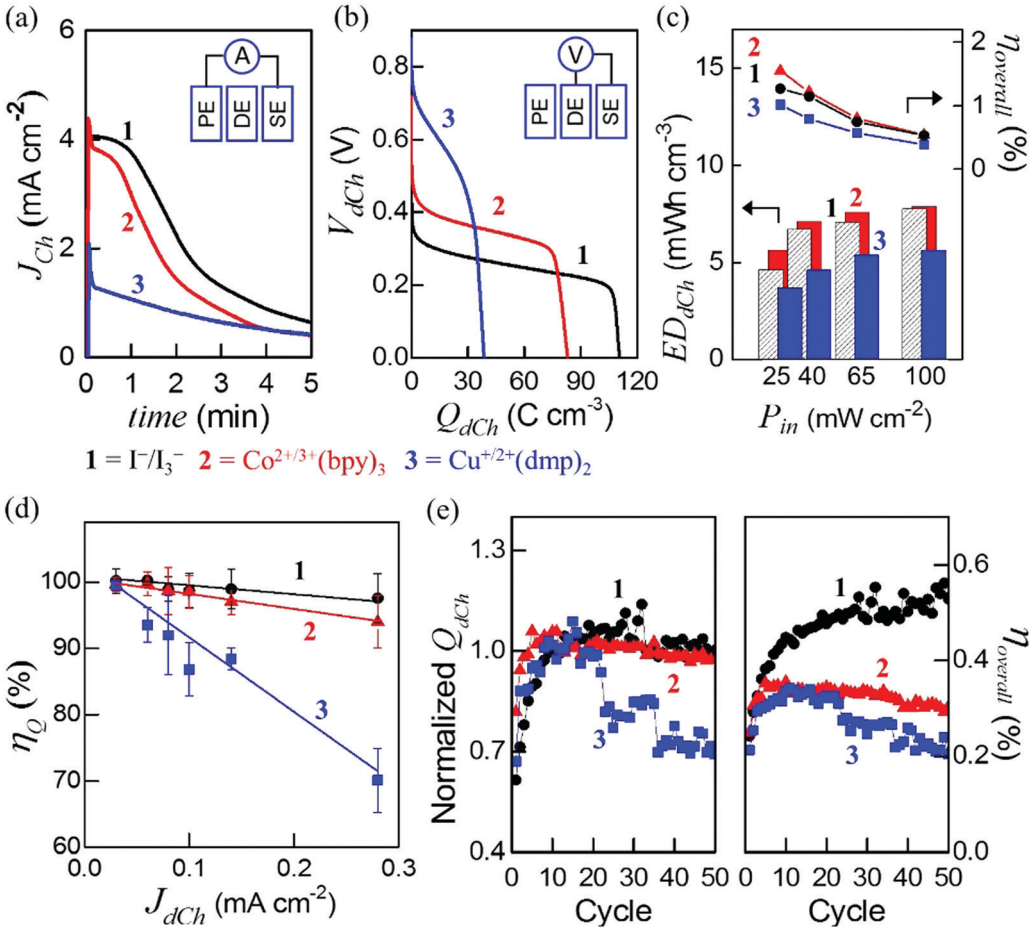

Fig. 2 DSPB charged at one sun irradiation. 1 (black) = I^-/I_3^-; 2 (red) = $Co^{2+/3+}(bpy)_3$; 3 (blue) = $Cu^{+/2+}(dmp)_2$. (a) Photo-charging profiles for 5 min at one sun (100 mW cm^{-2}). Currents were measured between PE and SE. (b) Galvanostatic discharging profiles at −0.03 mA cm^{-2}. Cell potentials were measured between DE and SE. (c) Light-to-charge energy efficiency ($\eta_{overall}$) and energy density (ED_{dCh}) galvanostatically discharged at various light intensity (P_{in}). (d) Dependency of η_Q on discharge rates. The average values of five discharge runs are shown with standard deviation (n = 5). (e) Capacity retention of DSPBs during cycles of photo-charging at 100 mW cm^{-2} for 5 min and discharging at −0.03 mA cm^{-2} up to 1 mV.

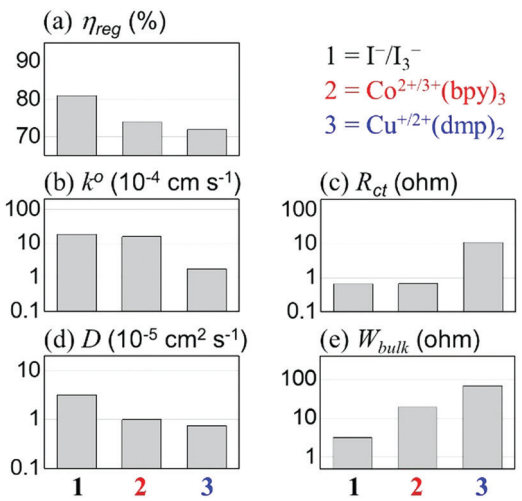

Fig. 3 Kinetic parameters. (a) Dye regeneration efficiency of mediator (η_{reg}). (b) Standard rate constant of charge transfer processes (k^0). (c) Charge transfer resistance (R_{ct}). (d) Ionic diffusion coefficient (D). (e) Warburg impedance (W_{bulk}).

81%, followed by $Co^{2+/3+}(bpy)_3$ at 74% and $Cu^{+/2+}(dmp)_2$ at 72%, which is consistent with the mediator-dependency of capacity. The η_{reg} was closely correlated with (1) the charge transfer kinetics (represented by the standard rate constant, k^0, and the charge transfer resistance, R_{ct}) and (2) the mass transfer kinetics (the ionic diffusion coefficient, D, and the Warburg impedance, W_{bulk}).[45–47] I^-/I_3^- showed the highest k^0 (1.9×10^{-3} cm s^{-1}) and D (3.2×10^{-5} cm^2 s^{-1}) and the lowest R_{ct} (0.66 Ω) and W_{bulk} (3.13 Ω), followed by $Co^{2+/3+}(bpy)_3$ and $Cu^{+/2+}(dmp)_2$. The kinetic limitation was shown clearly when photo-charging light intensities and discharge rates were controlled. The photo-charged capacities of $Cu^{+/2+}(dmp)_2$ were relatively independent of light intensity variations while that of I^-/I_3^- and $Co^{2+/3+}(bpy)_3$ increased with increasing light power (Fig. S5, ESI†). In the same vein, the mediator of the most sluggish kinetics ($Cu^{+/2+}(dmp)_2$) showed a significant decrease of η_Q with increasing discharge current while the η_Q of the others did not change significantly with discharge rates (Fig. 2d).

Capacity durability was investigated during the repeated photo-charge/galvanostatic discharge cycles (Fig. 2e). An initial

increase in Q_{dCh} was observed for all tested mediators, which indicates that the SE is possibly responsible for the increase. The poly-crystalline-characteristic surface of LMO@Gn particles having several nm grains evolved to 100 nm-scale single-crystal nanoparticles during the repeated charge/discharge cycles (Fig. S9, ESI†). The nanoparticles were well conjugated to each other, showing close interparticular contacts but clear boundaries. The bigger size of the crystalline domain (from 10^0 nm to 10^2 nm) decreases the tortuosity of lithium ion pathways while the well-contacted interparticular boundary possibly provides highways for lithium ion transport. The lithium ion pathways developed during the initial cycles make the intrinsic capacity of LMO more realized in effect.[35] The I^-/I_3^--containing cell showing the largest increase of Q_{dCh} required the longest duration of the LMO morphology transition before reaching the saturated capacity (Fig. 2e). Both I^-/I_3^- and $Co^{2+/3+}(bpy)_3$ exhibited stable capacity (Q_{dCh}) retention during cycles while the Q_{dCh} and $\eta_{overall}$ decreased significantly during cycles in the presence of the kinetically slow $Cu^{+/2+}(dmp)_2$. The instability of cycle retention of $Cu^{+/2+}(dmp)_2$ cells was more emphasized when the charge-to-discharge efficiency (η_Q) was considered instead of the overall efficiency (Fig. S10, ESI†). Both I^-/I_3^- and $Co^{2+/3+}(bpy)_3$ exhibited near 100% η_Q during all cycles except for several initial cycles. However, the slow kinetics of $Cu^{+/2+}(dmp)_2$ did not guarantee stable capacity retention.

Indoor lighting harvest and storage

The sluggish kinetics of $Cu^{+/2+}(dmp)_2$ limited the capacities (Q_{Ch} and Q_{dCh}) at one sun irradiation even if $Cu^{+/2+}(dmp)_2$ has the thermodynamic benefit of the most positive reduction potential. The merit of $Cu^{+/2+}(dmp)_2$ could be revived in a slow-charging situation. The indoor light intensity of bedrooms and study rooms is 300 to 600 lux and 500 to 1000 lux, respectively, which are less than 0.5% one sun illumination.[48–50] The DSPBs were tested at light intensities less than 0.60 mW cm^{-2} (2000 lux) by using a light emitting diode (LED) (Fig. S11, ESI†).[51,52] They were photo-charged for 10 min as the optimized photo-exposed time that was chosen from the photo-charging time dependency of the overall energy efficiency ($\eta_{overall}$) of

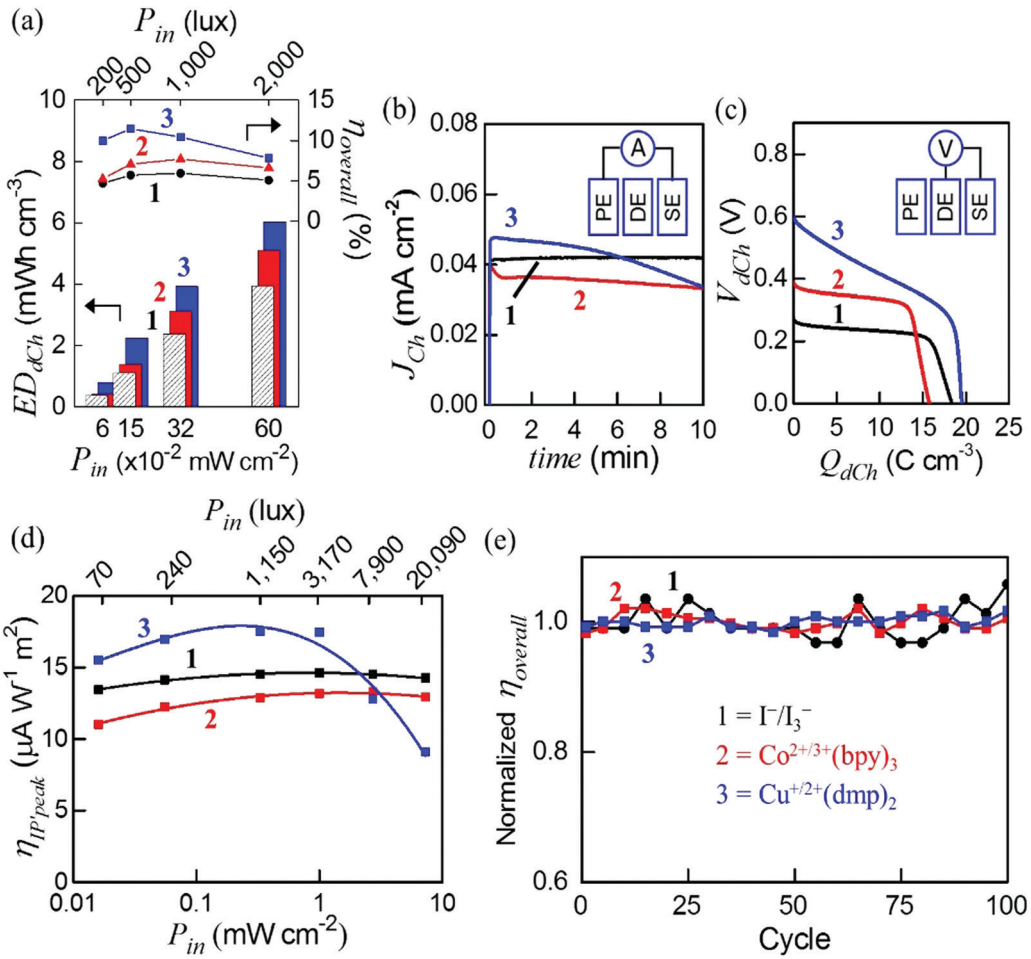

Fig. 4 Dim-light harvesting. (a) Light-to-charge energy efficiency ($\eta_{overall}$) and energy density (ED_{dCh}) galvanostatically discharged at various light intensity (P_{in}). (b) Photo-charging profiles of harvesting energy from a commercial white LED light source (P_{in} = 0.15 mW cm^{-2}). (c) Galvanostatically-discharging profiles at −3 μA cm^{-2}. (d) Maximum light-power-to-photo-current efficiency ($\eta_{IP}'_{peak}$; $\eta_{IP} = I_{sc,PE-DE}/P_{in}$; $I_{sc,PE-DE}$ = the short circuit current between PE and DE, P_{in} = the incident light power). (e) The $\eta_{overall}$ durability of DSPBs under dim light of a compact fluorescent lamp (P_{in} = 0.24 mW cm^{-2}).

$Cu^{+/2+}(dmp)_2$-containing cells (Fig. S12, ESI†). To achieve a high $\eta_{overall}$, shorter photo-charging times of less than 5 min were preferred at a higher illuminance of 1000 to 2000 lux. However, a photo-charging duration longer than 7 min was required at a lower illuminance of 200 to 500 lux. The photo-charging duration of 10 min was chosen for focusing on dim-light applications. At low light powers, interestingly, the kinetically-slowest $Cu^{+/2+}(dmp)_2$ showed a higher $\eta_{overall}$ than the kinetically-faster I^-/I_3^- and $Co^{2+/3+}(bpy)_3$ (Fig. 4a; η_{PCE} and $\eta_{storage}$ in Fig. S6, ESI†). The $\eta_{overall}$ at 11.5% obtained from $Cu^{+/2+}(dmp)_2$ at 0.15 mW cm^{-2} (500 lux) for 10 min charging is considered to be a very high efficiency, being four times as large as the $\eta_{overall}$ at 2.9% obtained from the supercapacitor wire-connected to an organic solar cell at 340 lux (2.9% for 52 min charging or 1.2% for 15 min charging[53]). To the best of our knowledge, the DSPB of this work is the first reported single-structured PRB successfully operated by an indoor light source (Fig. S13, ESI†).

The superiority of $Cu^{+/2+}(dmp)_2$ especially under dim-light conditions could be understood from a kinetic standpoint. The photo-charging process is not limited kinetically anymore in dim-light situations because the photo-stimulating power is too low to reach the kinetic limitation. The gaps of the initial J_{Ch} between kinetically fast and slow mediators were significantly large at one sun (Fig. 2a). Under dim-light conditions, however, the J_{Ch} of all mediators became similar with the gaps reduced. In the initial period of photo-charging, the kinetically-slow $Cu^{+/2+}(dmp)_2$ even overwhelmed the kinetically-fast I^-/I_3^- in terms of J_{Ch} (Fig. 4b). In the same vein, the maximum efficiency of light-power-to-photo-current ($\eta_{IP}{}'_{peak}$)[54] of the $Cu^{+/2+}(dmp)_2$ cell was estimated to be higher than those of other mediators specifically at low light intensities less than 1 mW cm^{-2} (Fig. 4d). Therefore, a similarly identical amount of charge (Q_{Ch}) was stored independent of the mediator under dim-light conditions. The thermodynamic benefit of a more-positive-reduction-potential mediator leads to higher ED_{dCh} because a similar amount of charge is released at a higher cell voltage during discharge (Fig. 4c). Photo-charge/galvanostatic discharge profiles under indoor light evidently supported the superiority of $Cu^{+/2+}(dmp)_2$ under dim light conditions (Fig. S14, ESI†). The difference of capacities between mediators became gradually negligible as the illuminance decreased from 2000 lux to 200 lux. Consequently, a higher V_{dCh} of $Cu^{+/2+}(dmp)_2$ led to a higher ED_{dCh}, confirming the thermodynamic gain. Therefore, the cell voltage was considered as the dominant factor that was more important than charge regeneration kinetics of mediators from the viewpoint of indoor energy harvesting.

We successfully operated a melody kit and an IoT device by using the DSPBs based on $Cu^{+/2+}(dmp)_2$ after photo-charging under commercial indoor light sources (compact fluorescent lamp and LED; Fig. S11c; refer to the ESI† video clips and Fig. S15 for details). Multiple DSPB cells were connected in series to meet the operating voltage of the devices (>3.5 V). The decrease in $\eta_{overall}$ of $Cu^{+/2+}(dmp)_2$ during the cycle observed at one sun (Fig. 2e) was not found under low-intensity light (Fig. 4e).

Conclusions

An external-power-free single-structured PRB, named a DSPB, was developed and its operation under indoor light was successfully demonstrated. The DSPB was designed (1) to harvest light energy by a dye and then (2) to store the harvested energy by oxidizing a redox mediator on the photo-electrode (PE) and reducing the other redox-active species (LMO@Gn) on the storage electrode (SE). Over-lithiation of LMO@Gn ($LiMn_2O_4 + Li^+ + e^- \rightarrow Li_2Mn_2O_4$) was carefully selected as the energy storage process on the SE, satisfying the requirements of the reduction process at the potential more negative than the potential of the mediators. Different from the high-power irradiation cases, the kinetics of charge and mass transfer of mediators did not limit the overall process in dim-light situations so that the thermodynamically-favorable and therefore more-positive-reduction-potential mediator was preferred without the kinetic consideration. The high-voltage copper complex mediator ($Cu^{+/2+}(dmp)_2$) was superior to the kinetically-fast but thermodynamically-unfavorable (more negative reduction potential) iodine mediator (I^-/I_3^-) in terms of photo-charging energy density and overall efficiency.

Conflicts of interest

There are no conflicts to declare.

Acknowledgements

This work was supported by NRF (Climate: 2016M1A2A2940910, 2017M1A2A2087813, 2017M3A7B4052802 and 2019M1A2A2065614), the Korea Institute of Energy Technology Evaluation and Planning (20183010013900), MOTIE (Open Lab: P0002068) and the 2018 UNIST Research Fund (1.190004.01), Korea.

References

1 Q. Li, Y. Liu, S. Guo and H. Zhou, *Nano Today*, 2017, **16**, 46–60.
2 S. Yun, Y. Qin, A. R. Uhl, N. Vlachopoulos, M. Yin, D. Li, X. Han and A. Hagfeldt, *Energy Environ. Sci.*, 2018, **11**, 476–526.
3 A. P. Cohn, W. R. Erwin, K. Share, L. Oakes, A. S. Westover, R. E. Carter, R. Bardhan and C. L. Pint, *Nano Lett.*, 2015, **15**, 2727–2731.
4 W. Guo, X. Xue, S. Wang, C. Lin and Z. L. Wang, *Nano Lett.*, 2012, **12**, 2520–2523.
5 S. Helal, W. Mann, H. El-Zabadani, J. King, Y. Kaddoura and E. Jansen, *Computer*, 2005, **38**, 50–60.
6 A. Nasiri, S. A. Zabalawi and G. Mandic, *IEEE Trans. Ind. Electron.*, 2009, **56**, 4502–4509.
7 R. Haight, W. Haensch and D. Friedman, *Science*, 2016, **353**, 124–125.
8 F. De Rossi, T. Pontecorvo and T. M. Brown, *Appl. Energy*, 2015, **156**, 413–422.

9 M. Freitag, J. Teuscher, Y. Saygili, X. Zhang, F. Giordano, P. Liska, J. Hua, S. M. Zakeeruddin, J.-E. Moser and M. Grätzel, *Nat. Photonics*, 2017, **11**, 372–378.
10 Y. S. Tingare, N. S. n. Vinh, H. H. Chou, Y. C. Liu, Y. S. Long, T. C. Wu, T. C. Wei and C. Y. Yeh, *Adv. Energy Mater.*, 2017, **7**, 1700032.
11 M. A. Mahmoudzadeh, A. R. Usgaocar, J. Giorgio, D. L. Officer, G. G. Wallace and J. D. W. Madden, *J. Mater. Chem. A*, 2016, **4**, 3446–3452.
12 J. Azevedo, T. Seipp, J. Burfeind, C. Sousa, A. Bentien, J. P. Araújo and A. Mendes, *Nano Energy*, 2016, **22**, 396–405.
13 N. F. Yan, G. R. Li and X. P. Gao, *J. Electrochem. Soc.*, 2014, **161**, A736–A741.
14 Y. Saito, S. Uchida, T. Kubo and H. Segawa, *ECS Trans.*, 2009, **16**, 27–34.
15 H. Nagai and H. Segawa, *Chem. Commun.*, 2004, 974–975, DOI: 10.1039/b400439f.
16 C. M. Hayner, X. Zhao and H. H. Kung, *Annu. Rev. Chem. Biomol. Eng.*, 2012, **3**, 445–471.
17 M. Yu, W. D. McCulloch, Z. Huang, B. B. Trang, J. Lu, K. Amine and Y. Wu, *J. Mater. Chem. A*, 2016, **4**, 2766–2782.
18 A. Gurung and Q. Qiao, *Joule*, 2018, **2**, 1217–1230.
19 J. Xu, Y. Chen and L. Dai, *Nat. Commun.*, 2015, **6**, 8103.
20 X. Xu, S. Li, H. Zhang, Y. Shen, S. M. Zakeeruddin, M. Graetzel, Y.-B. Cheng and M. Wang, *ACS Nano*, 2015, **9**, 1782–1787.
21 A. Gurung, K. Chen, R. Khan, S. S. Abdulkarim, G. Varnekar, R. Pathak, R. Naderi and Q. Qiao, *Adv. Energy Mater.*, 2017, **7**, 1602105.
22 C. Li, S. Cong, Z. Tian, Y. Song, L. Yu, C. Lu, Y. Shao, J. Li, G. Zou, M. H. Rümmeli, S. Dou, J. Sun and Z. Liu, *Nano Energy*, 2019, **60**, 247–256.
23 M. Yu, X. Ren, L. Ma and Y. Wu, *Nat. Commun.*, 2014, **5**, 5111.
24 M. Yu, W. D. McCulloch, D. R. Beauchamp, Z. Huang, X. Ren and Y. Wu, *J. Am. Chem. Soc.*, 2015, **137**, 8332–8335.
25 Q. Li, N. Li, Y. Liu, Y. Wang and H. Zhou, *Adv. Energy Mater.*, 2016, **6**, 1600632.
26 G. Nikiforidis, K. Tajima and H. R. Byon, *ACS Energy Lett.*, 2016, **1**, 806–813.
27 J. Lv, Y. X. Tan, J. Xie, R. Yang, M. Yu, S. Sun, M. D. Li, D. Yuan and Y. Wang, *Angew. Chem., Int. Ed.*, 2018, **130**, 12898–12902.
28 H. N. Tsao, C. Yi, T. Moehl, J. H. Yum, S. M. Zakeeruddin, M. K. Nazeeruddin and M. Grätzel, *ChemSusChem*, 2011, **4**, 591–594.
29 Y. Hao, Y. Saygili, J. Cong, A. Eriksson, W. Yang, J. Zhang, E. Polanski, K. Nonomura, S. M. Zakeeruddin and M. Gratzel, *ACS Appl. Mater. Interfaces*, 2016, **8**, 32797–32804.
30 A. Hagfeldt, G. Boschloo, L. Sun, L. Kloo and H. Pettersson, *Chem. Rev.*, 2010, **110**, 6595–6663.
31 J. B. Goodenough and K.-S. Park, *J. Am. Chem. Soc.*, 2013, **135**, 1167–1176.
32 W. Wang, Q. Luo, B. Li, X. Wei, L. Li and Z. Yang, *Adv. Funct. Mater.*, 2013, **23**, 970–986.
33 S. Liao, X. Zong, B. Seger, T. Pedersen, T. Yao, C. Ding, J. Shi, J. Chen and C. Li, *Nat. Commun.*, 2016, **7**, 11474.
34 S.-H. Kang, J. B. Goodenough and L. K. Rabenberg, *Chem. Mater.*, 2001, **13**, 1758–1764.
35 H. K. Noh, H.-S. Park, H. Y. Jeong, S. U. Lee and H.-K. Song, *Angew. Chem., Int. Ed.*, 2014, **53**, 5059–5063.
36 S. A. Sapp, C. M. Elliott, C. Contado, S. Caramori and C. A. Bignozzi, *J. Am. Chem. Soc.*, 2002, **124**, 11215–11222.
37 G. Boschloo and A. Hagfeldt, *Acc. Chem. Res.*, 2009, **42**, 1819–1826.
38 B. M. Klahr and T. W. Hamann, *J. Phys. Chem. C*, 2009, **113**, 14040–14045.
39 Y. Bai, Q. Yu, N. Cai, Y. Wang, M. Zhang and P. Wang, *Chem. Commun.*, 2011, **47**, 4376–4378.
40 M. Freitag, Q. Daniel, M. Pazoki, K. Sveinbjörnsson, J. Zhang, L. Sun, A. Hagfeldt and G. Boschloo, *Energy Environ. Sci.*, 2015, **8**, 2634–2637.
41 C. M. Julien, A. Mauger, K. Zaghib and H. Groult, *Inorg.*, 2014, **2**, 132–154.
42 C. Liu, Z. G. Neale and G. Cao, *Mater. Today*, 2016, **19**, 109–123.
43 W. Li, H. C. Fu, L. Li, M. Cabán-Acevedo, H. He Jr and S. Jin, *Angew. Chem., Int. Ed.*, 2016, **55**, 13104–13108.
44 A. Yella, H.-W. Lee, H. N. Tsao, C. Yi, A. K. Chandiran, M. K. Nazeeruddin, E. W.-G. Diau, C.-Y. Yeh, S. M. Zakeeruddin and M. Grätzel, *Science*, 2011, **334**, 629–634.
45 M. K. Kashif, J. C. Axelson, N. W. Duffy, C. M. Forsyth, C. J. Chang, J. R. Long, L. Spiccia and U. Bach, *J. Am. Chem. Soc.*, 2012, **134**, 16646–16653.
46 Z. Sun, M. Liang and J. Chen, *Acc. Chem. Res.*, 2015, **48**, 1541–1550.
47 J. Wu, Z. Lan, J. Lin, M. Huang, Y. Huang, L. Fan and G. Luo, *Chem. Rev.*, 2015, **115**, 2136–2173.
48 A. Pears, *Strategic study of household energy and greenhouse issues*, Sustainable Solutions Pty Ltd, 1998.
49 D. H. Li, T. N. Lam and S. Wong, *Energy Convers. Manage.*, 2006, **47**, 1133–1145.
50 Y.-W. Bai and Y.-T. Ku, *IEEE Trans. Consum. Electr.*, 2008, **54**, 1173–1176.
51 M. Freunek, M. Freunek and L. M. Reindl, *IEEE J. Photovolt.*, 2013, **3**, 59–64.
52 B. Minnaert and P. Veelaert, *Energies*, 2014, **7**, 1500–1516.
53 B. P. Lechêne, M. Cowell, A. Pierre, J. W. Evans, P. K. Wright and A. C. Arias, *Nano Energy*, 2016, **26**, 631–640.
54 B.-M. Kim, H.-G. Han, J. S. Kim, H. Shin and T.-H. Kwon, *ACS Appl. Mater. Interfaces*, 2017, **9**, 2572–2580.